

Coexistence of Anderson-Bogoliubov phonon and quadrupole cluster vibration in neutron star inner crust

Tsunenori Inakura^{1,2} and Masayuki Matsuo¹

¹*Department of Physics, Faculty of Science, Niigata University, Niigata 950-2181, Japan*

²*Laboratory for Advanced Nuclear Energy, Institute of Innovative Research, Tokyo Institute of Technology, Tokyo 152-8550, Japan*

Background: Low-lying collective excitations of inner crust matter in neutron stars are expected to have impact on observables such as the quasi-periodic oscillation in giant flares and the cooling of inner crust in transient phenomena. Coupling between Anderson-Bogoliubov superfluid phonon (AB phonon) in superfluid neutron gas and collective excitations of nuclear clusters is a key issue.

Purpose: We intend to predict the nature of low-lying excitation modes of superfluid inner crust matter with focus on quadrupole excitations around a spherical nuclear cluster. We study how the AB phonon of neutron superfluid and possible quadrupole shape vibration of clusters are affected by the inhomogeneous structure of inner crust matter.

Methods: The coordinate-space Hartree-Fock-Bogoliubov method and the quasiparticle random-phase approximation formulated in a spherical Wigner-Seitz cell are adopted to describe neutron superfluidity and low-lying collective excitations. We perform systematic numerical calculations for quadrupole excitations by varying the neutron chemical potential and the number of protons in a cell.

Results: The calculated results indicate emergence of both AB phonon and quadrupole shape vibration of the cluster with small mixing between the two collective modes. The quadrupole AB phonon is similar to that in uniform superfluid apart from small admixture of the shape vibration of cluster. The excitation energy and the collectivity of the cluster vibration mode shows strong and oscillatory dependence on the neutron chemical potential (the neutron gas density), leading to softening and instability in certain situations. This is caused by the resonance shell effect where unbound but resonant single-particle states of neutrons play a central role.

Conclusions: The AB phonon of superfluid neutron gas and the quadrupole shape vibration of nuclear cluster coexist in inner crust. The coupling between the AB phonon and the quadrupole shape vibration is weak. The collectivity of the quadrupole shape vibration is governed by the resonance shell effect, and it suggests that emergence of deformed nuclear clusters is possible at any layer of inner crust.

I. INTRODUCTION

Nuclear matter in the inner crust of neutron stars consists of a lattice of nuclear clusters immersed in superfluid neutron gas[1–3]. The coexistence of nuclear clusters and superfluid neutrons brings about rich many-body phenomena. A typical example might be the pinning and unpinning of superfluid vortices, which is considered to be responsible for the glitch in the rotation frequency of a neutron star[4–6]. Another interest is found in collective excitations of inner crust matter. The lattice vibration, the collective displacement motion of nuclear clusters, may be microscopic entity of the seismic oscillation observed as the quasi-periodic oscillation in the giant flares[7–9]. Recently the superfluid phonon[10–12], called also the Anderson-Bogoliubov phonon, attracts new attentions[13–20]. It may influence the heat capacity (due to this additional degrees of freedom)[20, 21], the seismic oscillation (through the coupling between the superfluid and the lattice phonons)[14, 17], and the thermal conductivity (as a new heat carrier)[13–16]. Possibility of forming a exotic crystalline structure is also suggested[18, 19]. The coupling between the nuclear cluster and the superfluid phonon is regarded as a key issue in these studies.

Theoretical approaches to the collective excitation of

inner crust matter have been undertaken in two different directions. One is macroscopic approaches focusing on low-frequency limit[13–19, 22, 23], where the collective degrees of freedom of the superfluid phonon is explicitly introduced in the thermodynamic limit or in the hydrodynamic framework while the nucleon degrees of freedom are treated implicitly. Another is microscopic approaches based on the many-body quantum mechanics for interacting nucleons. In the latter direction the linear response methods (the quasiparticle random phase approximation QRPA) based on nuclear density functional models or the Hartree-Fock-Bogoliubov (HFB) models are often adopted[20, 21, 24–26]. Properties of the superfluid phonon mode are studied in detail within the QRPA for pure and uniform neutron superfluid[20]. However, if one intends to describe the inhomogeneous system consisting of nuclear cluster and neutron superfluid, one resorts to QRPA calculations assuming a spherical Wigner-Seitz cell enclosing a single cluster[21, 24–26]. In a preceding publication (Part I hereafter)[26] we have studied along this line the dipole excitation in the cell since the displacement motion of cluster has the multipole $L = 1$ and the dipole channel is responsible for the coupling between the superfluid phonon and the lattice phonon. This study predicts that the superfluid phonon with the dipole multipolarity is influenced strongly by

the presence of cluster in such a way that the amplitude of superfluid phonon is significantly hindered inside the nuclear cluster. This result suggests that the coupling between the superfluid phonon and the displacement motion of cluster (i.e. the lattice phonon) might be weak, implying possible enhancement of the thermal conductivity of the inner crust.

In the present work we analyze the quadrupole excitation in the spherical Wigner-Seitz cell of inner crust with use of the same model as that in Part I. In a pioneering work by Khan et al., where a HFB plus QRPA model is applied to quadrupole excitations, a low-lying collective mode called the supergiant resonance is predicted[21]. Its relation to the superfluid phonon is suggested, but only in a qualitative argument. In another study using a Hartree-Fock plus RPA, in which the nucleon pair correlation is neglected and the superfluid phonon is not expected, low-lying collective modes with a character of the multipole shape vibration of cluster are predicted[25]. Because of this situation, a consistent picture is not obtained yet and questions and problems remain. What is the relation among the superfluid phonon, the supergiant resonance in Khan et al.[21] and the shape vibration of cluster? How is the superfluid phonon affected by the presence of cluster? Is there difference between the dipole and quadrupole modes of the superfluid phonon? Does the cluster shape vibration exist or how is it affected when it is immersed in superfluid neutron gas? The purposes of the present study is to answer these questions. In short, we intend to clarify the nature of the low-lying excitation modes of superfluid inner crust matter with focus on quadrupole excitations around a spherical nuclear cluster.

In the following we call the superfluid phonon mode of neutron superfluid the Anderson-Bogoliubov phonon mode (abbreviated as AB phonon) to keep the same nomenclature as in Part I[26]. The paper is organized as follows: In Sec. II, we briefly explain the model we use to describe the ground state and the excitation modes of inner crust matter in the Wigner-Seitz approximation. In Sec. III, we show numerical results of the QRPA calculation performed for the quadrupole excitations in the spherical Wigner-Seitz cell. We will show that there emerge two low-lying collective excitations, which are related to both the AB phonon mode of superfluid neutron gas and the quadrupole shape vibration of the nuclear cluster. We will investigate in detail basic properties of these low-lying collective modes to clarify the interplay between the AB phonon mode and the shape vibration of cluster. It will be turned out that the quadrupole shape collectivity of the cluster exhibits a peculiar shell effect which arises not from neutrons bound to clusters, but from unbound neutrons permeating the nuclear cluster and neutron gas. Sec. IV is devoted to the conclusion.

II. MODEL

We employ the HFB model and the QRPA theory. The calculation framework and the model parameters are the same as those in Part I[26]. Here we recapitulate the adopted HFB+QRPA formalism briefly. For other details, we refer the readers to Refs. [26–30].

To calculate the properties of the inner crust, we introduce the spherical Wigner-Seitz approximation with a Wigner-Seitz radius of $R_{\text{WS}} = 20$ fm. Following the standard prescriptions adopted in the HF/HFB calculations[31–39], we impose the von-Neumann-Dirichlet boundary condition[31]. Nucleon configuration of the Wigner-Seitz cell is specified with the neutron chemical potential (Fermi energy) λ_n and a fixed integer number Z of protons in the cell.

The ground state configuration of inner crust matter for given Z and λ_n is obtained by solving the HFB equation in the coordinate representation. We adopt the zero-range effective Skyrme SLy4 interaction [40] for the Hartree-Fock potential (in the particle-hole channel). A version of density-dependent delta interaction [41, 42] is used to obtain the pairing potential (in the pairing channel)

$$\Delta_\tau(\mathbf{r}) = V_{\text{pair}} \left[1 - \eta \left(\frac{\rho_\tau(\mathbf{r})}{\rho_c} \right)^\alpha \right] \tilde{\rho}_\tau(\mathbf{r}) \quad (1)$$

and the pair density

$$\tilde{\rho}_\tau(\mathbf{r}) = \langle \Psi_0 | \psi(\mathbf{r} \uparrow) \psi(\mathbf{r} \downarrow) | \Psi_0 \rangle. \quad (2)$$

Here $\tau = n, p$ denotes isospin, \uparrow and \downarrow are up and down components of spin σ , and $\rho_c = 0.08 \text{ fm}^{-3}$. We set the cut-off $j_{\text{max}} = (75/2)\hbar$ for the single-particle partial waves and we include all the quasiparticle states under the cut-off quasiparticle energy $E_{\text{cut}} = 60$ MeV. To characterize the neutron superfluid outside the nuclear cluster we evaluate its average neutron density and average pair potential as

$$\rho_{\text{ext}} = \frac{\int_{R_1}^{R_2} dr r^2 \rho_n(r)}{\int_{R_1}^{R_2} dr r^2}, \quad \Delta_{\text{ext}} = \frac{\int_{R_1}^{R_2} dr r^2 \Delta_n(r)}{\int_{R_1}^{R_2} dr r^2} \quad (3)$$

with $R_1 = 12$ fm and $R_2 = 18$ fm.

The QRPA calculation is performed on top of the HFB ground state Ψ_0 . In the present study we focus on the quadrupole excitations. We utilize the linear response formalism [27–29] for the QRPA. We describe responses of the system with respect to the quadrupole operator Q , and the pair addition and removal operators, P_{add} and P_{rm} , defined by

$$\begin{aligned} Q &= \sum_{\sigma} \int d\mathbf{r} r^2 Y_{2M}(\hat{\mathbf{r}}) \psi^\dagger(\mathbf{r}\sigma) \psi(\mathbf{r}\sigma), \\ P_{\text{add}} &= \int d\mathbf{r} Y_{2M}(\hat{\mathbf{r}}) \psi^\dagger(\mathbf{r}\downarrow) \psi^\dagger(\mathbf{r}\uparrow), \\ P_{\text{rm}} &= \int d\mathbf{r} Y_{2M}(\hat{\mathbf{r}}) \psi(\mathbf{r}\uparrow) \psi(\mathbf{r}\downarrow). \end{aligned} \quad (4)$$

We solve the QRPA linear response equations for fluctuations of the nucleon density $\rho(\mathbf{r})$, the nucleon pair density $\tilde{\rho}(\mathbf{r})$ and its complex conjugate $\tilde{\rho}^*(\mathbf{r})$. The spectral representation is adopted for the density response function and all the quasiparticle states adopted in the HFB calculation are included. We calculate the strength function

$$S(O; E) = \sum_{Mi} \delta(E - E_i) \left| \langle \Psi_i^{2M} | \hat{O} | \Psi_0 \rangle \right|^2, \quad (5)$$

for the quadrupole excited states Ψ_i^{2M} with respect to the operators $\hat{O} = Q, P_{\text{add}}$ and P_{rm} of neutrons and protons separately. With a small imaginary constant ϵ in the energy argument, the delta function peaks in the strength functions are smeared with the Lorentzian function having the FWHM of 2ϵ . We evaluate the strength $B(O) = \sum_M \left| \langle \Psi_i^{2M} | \hat{O} | \Psi_0 \rangle \right|^2$ of each excited state by integrating the strength function in an energy interval $E \in [E_i - 10\epsilon, E_i + 10\epsilon]$ around its peak energy E_i . We employ $\epsilon = 10$ keV. Three transition densities from the HFB ground state Ψ_0 to the i th QRPA excited state Ψ_i^{2M} ,

$$\begin{aligned} \delta\rho_{\text{ph}}(\mathbf{r}) &= \langle \Psi_0 | \sum_{\sigma} \psi^{\dagger}(\mathbf{r}\sigma)\psi(\mathbf{r}\sigma) | \Psi_i^{2M} \rangle = Y_{2M}(\hat{\mathbf{r}})\delta\rho_{\text{ph}}(r), \\ \delta\tilde{\rho}_{\text{pp}}(\mathbf{r}) &= \langle \Psi_0 | \psi(\mathbf{r}\uparrow)\psi(\mathbf{r}\downarrow) | \Psi_i^{2M} \rangle = Y_{2M}(\hat{\mathbf{r}})\delta\tilde{\rho}_{\text{pp}}(r), \\ \delta\tilde{\rho}_{\text{hh}}(\mathbf{r}) &= \langle \Psi_0 | \psi^{\dagger}(\mathbf{r}\downarrow)\psi^{\dagger}(\mathbf{r}\uparrow) | \Psi_i^{2M} \rangle = Y_{2M}(\hat{\mathbf{r}})\delta\tilde{\rho}_{\text{hh}}(r), \end{aligned} \quad (6)$$

are obtained from the corresponding fluctuating densities at the peak energy E_i . Note that the calculated spectrum is discretized because of the boundary condition.

As the residual interaction which enters in the QRPA calculation, we adopt the same effective pairing interaction for the pairing channel. Concerning the residual interaction in the particle-hole channel, we adopt the Landau-Migdal approximation [28, 29, 43–45] with a renormalization scheme often employed in this approximation. Namely we replace the self-consistent particle-hole interaction v_{ph} by the Landau-Migdal interaction $f \times v_{\text{LM}}$ derived from the Skyrme interaction and renormalized with a factor f . The factor f is determined to bring a peak corresponding to the displacement motion to zero energy in the drip-line nucleus for a given Z . The same value of f is used for the Wigner-Seitz cells with the same Z .

III. RESULTS AND DISCUSSION

We have performed the HFB and QRPA calculations systematically for various configurations specified by the neutron chemical potential λ_n and the proton number Z , with changing Z and λ_n , in order to study basic properties of excitation modes of inner crust matter. The adopted proton numbers are $Z = 20, 28, 40$, and 50 , chosen to cover the range predicted in the previous HFB or HF calculations for the equilibrium [31, 35–37]. For

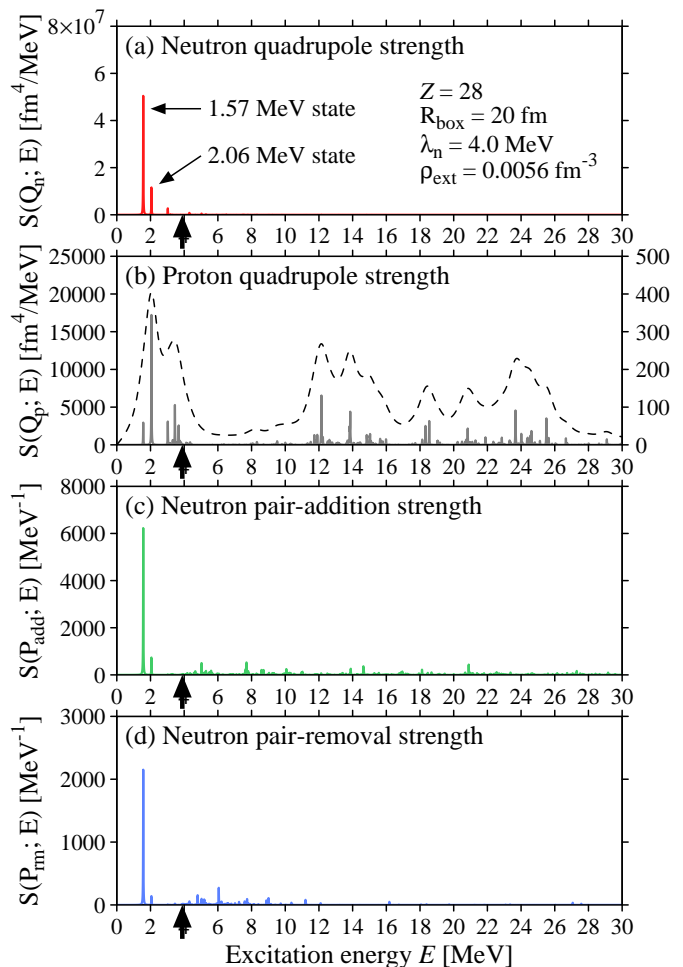


FIG. 1. (a) Strength function $S(Q_n; E)$ for neutron quadrupole operator, (b) $S(Q_p; E)$ for proton quadrupole operator, (c) $S(P_{\text{add}}; E)$ for neutron pair-addition operator and (d) $S(P_{\text{rm}}; E)$ for neutron pair-removal operator, calculated for $Z = 28$ system with $\lambda_n = 4.0$ MeV, plotted as a function of the excitation energy E . Arrows indicate the threshold energy $2\Delta_{\text{ext}}$. The smearing parameter is $\epsilon = 10$ keV. Dashed curve in (b) is the proton quadrupole strength function $S(Q_p; E)$ obtained with $\epsilon = 500$ keV (with the scale on the right axis).

the neutron chemical potential, we vary it in the range $\lambda_n = 1 - 6$ MeV, which corresponds to the density of neutron matter $\rho_n \approx 5 \times 10^{-4} - 1 \times 10^{-2} \text{ fm}^{-3}$. The ground states obtained by the HFB calculation are same as in Part I [26].

A. Low-lying quadrupole excitations

We first discuss the case of $Z = 28$ and $\lambda_n = 4.0$ MeV chosen as representative.

Figures 1(a)-(d) show the strength functions $S(O; E)$ for the neutron quadrupole moment, $O = Q_n$, the proton

quadrupole moment Q_p , the neutron pair-addition operator P_{add} and the neutron pair-removal operator P_{rm} , respectively, for the $Z = 28$ system with $\lambda_n = 4.0$ MeV. Two distinct peaks at $E = 1.57$ MeV and at $E = 2.06$ MeV are seen in the low-lying region. These peaks are located below $2\Delta_{\text{ext}}$ (twice of the neutron pair gap, indicated with arrows). Above this threshold energy, the QRPA excited states are densely distributed (and would become continuous if $R_{\text{WS}} \rightarrow \infty$). It is noted here that the peak at $E = 1.57$ MeV is significant in the strength functions for the neutron operators Q_n , P_{add} and P_{rm} , but not in the strength function for the proton operator Q_p . The second peak at $E = 2.06$ MeV, however, has the largest strength in the proton quadrupole moment Q_p , but the strengths for the neutron operators are much smaller than those of the first peak at $E = 1.57$ MeV. Apparently there exist two kinds of low-lying collective modes which have different characters.

Let us examine the peak at $E = 1.57$ MeV in detail. This state has the strengths $B(Q_n) = 1.49 \times 10^6 \text{ fm}^4$, $B(P_{\text{add}}) = 183$ and $B(P_{\text{rm}}) = 63$ for the neutron operators, which are the largest among the QRPA excited states and exhaust 67 %, 21 %, and 42 %, respectively, of the total strengths (non-energy-weighted sums integrated up to 50 MeV). Note that the neutron quadrupole strength $B(Q_n) = 1.49 \times 10^6 \text{ fm}^4$ is larger by a factor of 10^{2-3} than a typical value of the low-lying collective 2_1^+ state in isolated nuclei, $B(E2)/e^2 \sim 10B_{\text{W}}$ (B_{W} being the Weisskopf unit[46]). Having this extraordinary quadrupole strength, we consider that this state may correspond to what is called the supergiant quadrupole resonance in Khan et al.[21].

Figure 2(a) shows the neutron and proton particle-hole transition densities, $\delta\rho_{\text{ph}}^{\nu}(r)$ and $\delta\rho_{\text{ph}}^{\pi}(r)$, and the neutron pair-addition and -removal transition densities, $\delta\tilde{\rho}_{\text{pp}}^{\nu}(r)$ and $\delta\tilde{\rho}_{\text{hh}}^{\nu}(r)$, of the 1.57 MeV state. It is seen that the neutron particle-hole transition density $\delta\rho_{\text{ph}}^{\nu}(r)$ as well as the neutron pair-addition/removal transition densities, $\delta\tilde{\rho}_{\text{pp}}^{\nu}(r)$ and $\delta\tilde{\rho}_{\text{hh}}^{\nu}(r)$, have finite amplitudes in the whole region of neutron gas $r \gtrsim 6$ fm. This is the origin of the extremely large neutron strengths. The three transition densities far outside the nucleus $r \gtrsim 9$ fm exhibits a signature of the AB phonon mode: They share an approximate sinusoidal shape in the neutron gas region while the pair transition densities $\delta\tilde{\rho}_{\text{pp}}^{\nu}(r)$ and $\delta\tilde{\rho}_{\text{hh}}^{\nu}(r)$ have an opposite phase to one another[26]. The neutron and proton particle-hole transition densities $\delta\rho_{\text{ph}}^{\nu}(r)$ and $\delta\rho_{\text{ph}}^{\pi}(r)$, however, show enhanced amplitude in the surface region of the cluster, $4 \text{ fm} \lesssim r \lesssim 8 \text{ fm}$, with the phase coherence. This behaviour in the surface region is similar to the one known in the low-lying quadrupole shape oscillation of isolated nuclei.

The 2.06 MeV state is recognized in the proton quadrupole strength function, but it is hard to be seen in the neutron strength functions. The proton strength $B(Q_p) = 508 \text{ fm}^4$ of the 2.06 MeV state is the same order of magnitude as the typical $B(E2)$ values of the low-lying quadrupole vibration in isolated nuclei. (Note

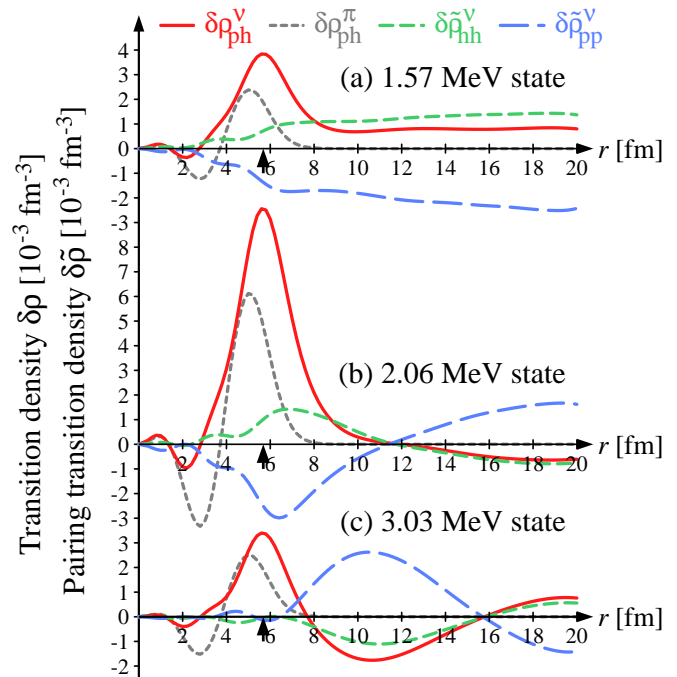


FIG. 2. Transition densities of the low-lying quadrupole collective modes whose excitation energies are (a) $E = 1.57$ MeV, (b) 2.06 MeV, and (c) 3.03 MeV, obtained for $Z = 28$ system with $\lambda_n = 4.0$ MeV. Red, gray, green, and blue curves are $\delta\rho_{\text{ph}}^{\nu}(r)$, $\delta\rho_{\text{ph}}^{\pi}(r)$, $\delta\tilde{\rho}_{\text{pp}}^{\nu}(r)$, and $\delta\tilde{\rho}_{\text{hh}}^{\nu}(r)$, respectively. The arrows indicate the surface position of the cluster[26]. See text for details.

$B(E2) = e^2 B(Q_p)$.) The neutron quadrupole strength $B(Q_n) = 3.46 \times 10^5 \text{ fm}^4$ is two orders of magnitude larger than those in isolated nuclei, but significantly smaller than that of the 1.57 MeV state. The transition densities of the 2.06 MeV state, shown in Fig. 2(b), displays a similar behavior as those of the 1.57 MeV state, but some difference is clearly seen: The neutron and proton particle-hole amplitudes around the cluster surface is much larger than those of the 1.57 MeV state and it suggests a closer relation to the quadrupole shape vibration of the cluster. The neutron amplitudes outside the cluster displays a node at $r \approx 12$ fm.

B. Coexistence of AB phonon and quadrupole cluster vibration

In order to investigate the characteristic features of these two collective excitations, we look into roles of the residual interaction. For this purpose we shall drop off some parts of the residual interaction which enters in the QRPA calculation. Figure 3 shows the strength functions $S(Q_n; E)$, $S(Q_p; E)$ and $S(P_{\text{add}}; E)$, 1) which are obtained using only the residual pairing interaction (i.e. the particle-hole part of the residual interaction is neglected) plotted with green curves, 2) those (blue curves)

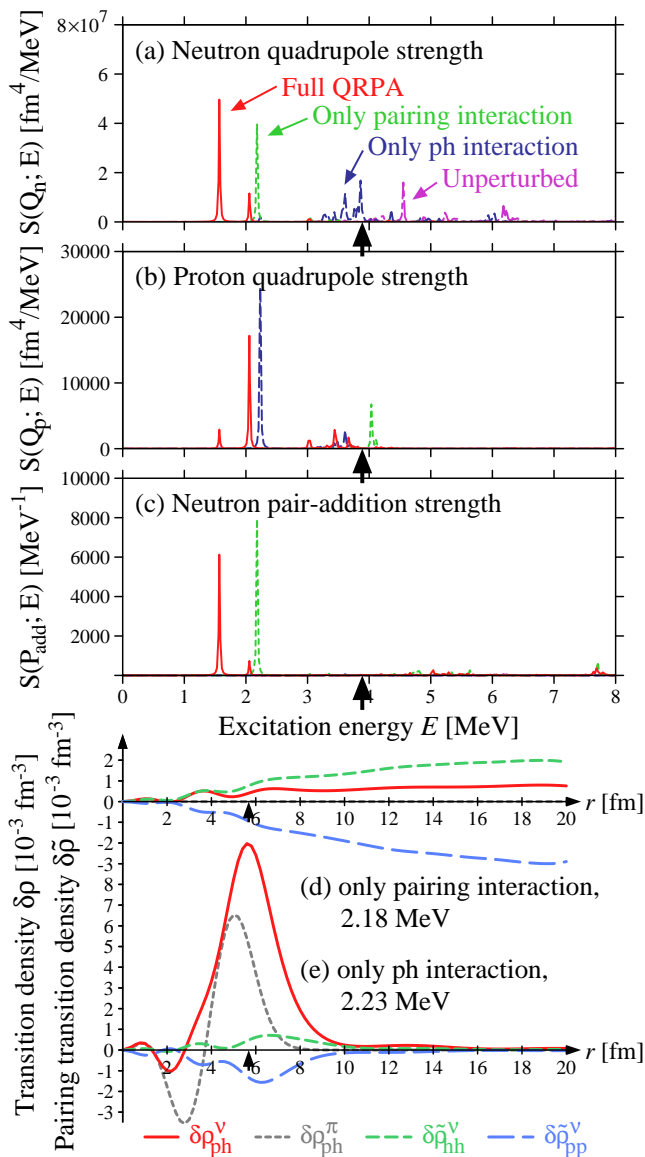


FIG. 3. Uppers: (a) Strength function $S(Q_n; E)$, (b) $S(Q_p; E)$, and (c) $S(P_{\text{add}}; E)$ calculated with the full residual interaction (red curve), with only the residual pairing interaction (green dashed), and with only the residual particle-hole interpretation (blue long-dashed). Unperturbed results (magenta long-dashed dotted) are also plotted. The system is $Z = 28$ and $\lambda_n = 4.0$ MeV. Lower: Transition densities of the low-lying collective mode obtained in calculations (d) with only residual pairing interaction and (e) with only the residual particle-hole interaction. Red, gray, green, and blue curves are $\delta\rho_{\text{ph}}^{\nu}(r)$, $\delta\rho_{\text{ph}}^{\pi}(r)$, $\delta\tilde{\rho}_{\text{hh}}^{\nu}(r)$, and $\delta\tilde{\rho}_{\text{pp}}^{\nu}(r)$, respectively. See also the captions of Figs. 1 and 2.

obtained with only the residual particle-hole interaction (the residual pairing interaction is neglected instead), and 3) unperturbed results (magenta curves) in which all the residual interactions are neglected. The obtained strengths functions are shown in the panels (a), (b) and (c). The calculation using only the residual pairing inter-

action produces a collective state which appears as a peak at 2.18 MeV with large neutron strengths. This state has apparent characters of the AB phonon mode as are seen in its transition densities, shown in Fig. 3(d): the oscillatory behavior with long wave length, $\delta\tilde{\rho}_{\text{hh}}^{\nu}(r) \sim A j_2(qr)$ and $\delta\tilde{\rho}_{\text{hh}}^{\nu}(r) \sim -A j_2(qr)$, is clearly seen, especially outside the nuclear cluster $r \gtrsim 8$ fm. When only the particle-hole interaction included (and the residual pairing interaction is neglected), the quadrupole shape vibration of the cluster emerges seen as a peak at 2.23 MeV in the proton strength function. In fact, transition densities of this state [Fig. 3(e)] exhibit clearly features of isoscalar quadrupole shape vibration of the cluster: The particle-hole transition densities $\delta\rho_{\text{ph}}^{\nu}(r)$ and $\delta\rho_{\text{ph}}^{\pi}(r)$ of neutrons and protons both have large amplitudes with the same phase around the surface region of the cluster, $4 \text{ fm} \lesssim r \lesssim 8 \text{ fm}$, while all the transition densities diminish outside the cluster $r \gtrsim 10 \text{ fm}$.

Having these observations, we can interpret the two excitation modes at $E = 1.57$ MeV and 2.06 MeV in the full QRPA calculation as mixtures or coupled modes of the AB phonon mode and the quadrupole shape vibration of the cluster. The transition densities of the 1.57 MeV state, Fig. 2(a), appear an in-phase superposition of those in Figs. 3(d) and (e) while the component of the AB phonon mode is dominant. The dominance of the AB phonon is seen also in the neutron strengths [Fig. 3(a)(c)], where the peak heights (red curves) are comparable to those of the pure AB phonon mode (green curves) obtained with only the pairing interaction. Therefore the 1.57 MeV state may be characterized as a AB-phonon-dominant mode. Concerning the 2.06 MeV state, on the other hand, the transition densities in Fig. 2(b) appear an approximate out-of-phase superposition of those in Fig. 3(d) and (e) while the component of the cluster shape vibration is dominant. Therefore it is characterized as a cluster-vibration-dominant mode. It is not surprising that the AB phonon mode of superfluid neutron gas and the shape vibration of the cluster couple with one another as the neutron gas and the nuclear cluster share the same nucleon degrees of freedom. In addition the low-lying shape vibration of nuclei is known to be influenced by the pair correlation, and hence the same is expected for the cluster shape vibration. A remarkable point here is that the characters of the AB phonon mode and the cluster shape vibration remain well in spite of the mixing. This suggests that the AB phonon mode and the cluster shape vibration coexist and the coupling between the two fundamental excitation modes is rather weak in the case of the quadrupole excitations. This is consistent with our finding in the dipole case[26], where weak coupling between the dipole AB phonon mode and the displacement motion of cluster is suggested.

We briefly mention other types of collective excitation modes which are identified in the present QRPA calculation. The third largest peak in the neutron quadrupole strength function [Fig. 1 (a)] has an excitation energy of 3.03 MeV. The transition densities of this state, shown

in Fig. 2(c), suggest that this state may be interpreted as the AB phonon mode of the second harmonics with one node at $r \approx 12$ fm with small mixing of the cluster shape vibration. A bunch of states around $E \approx 11$ to 16 MeV having significant proton quadrupole strength is a high-lying collective excitation of the cluster, which corresponds to the isoscalar giant quadrupole resonance in isolated nuclei. A distribution of the proton strengths around 25 MeV is an analog of the isovector giant quadrupole resonance. Detailed analysis of these collective excitations are out of scope of the present paper, and is left for future study.

We remark here relation between the low-lying collective excitation modes found in the present calculation and those discussed in the preceding works[21, 25]. Khan et al.[21] adopted the HFB plus QRPA model, which is similar to the present one. They discuss collective excitations in terms of the strength function for the isoscalar quadrupole operator $Q_{IS} = Q_n + Q_p$, and found a low-lying significant peak, named the supergiant resonance. We find in the present calculation that the isoscalar quadrupole strength function $S(Q_{IS}; E)$ looks similar to the neutron strength function $S(Q_n; E)$ when plotted in the same scale. (This is because the proton strength is smaller by a factor of 10^{-3} than the neutron strength, see Figs. 2(a) and (b).) Therefore the supergiant resonance of Khan et al.[21] may correspond to the AB-phonon-dominant mode in the present calculation. It is likely that the cluster-vibration-dominant mode is not visible in the analysis of Khan et al. due to their use of relatively large smoothing constant (150keV), which may hide a small peak nearby the large peak. Baroni et al. performed the HF plus RPA calculation, which neglects the nucleon pair correlation[25]. The HF plus RPA model predicts low-lying quadrupole shape vibration mode as well as the high-lying mode which corresponds to isoscalar giant quadrupole resonance of the cluster. The low-lying shape vibration mode in Ref. [25], however, exhibits some differences from the cluster-vibration-dominant mode in the present model: The former emerges as a bump of strength distribution while the latter is a single discrete state. These differences are attributed to the neutron pair correlation and the presence of the pair gap. Note also that due to the lack of the pair correlation the AB phonon mode is not expected to exist in Baroni et al. as we have seen in the reduced QRPA calculation including only the residual particle-hole interaction (blue curve) shown in Fig. 3.

C. Systematics

We shall discuss systematic behaviour of the two kinds of low-lying collective modes by varying λ_n and Z .

We first examine dependence on the neutron chemical potential λ_n . In Fig. 4 we plot the strength functions $S(Q_n; E)$, $S(Q_p; E)$, and $S(P_{\text{add}}; E)$ for $Z = 28$ systems with $\lambda_n = 1.0, 2.0, \dots, 6.0$ MeV. It is evident in the neu-

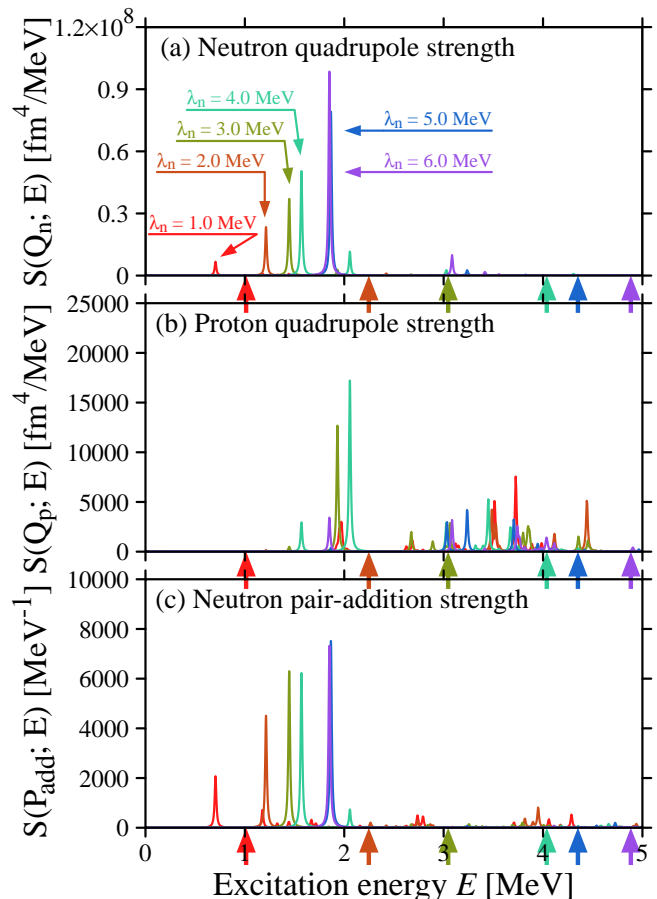


FIG. 4. Strength functions (a) $S(Q_n; E)$, (b) $S(Q_p; E)$, and (c) $S(P_{\text{add}}; E)$ for $Z = 28$ system with $\lambda_n = 1.0$ MeV (red curves), 2.0 MeV (brown), 3.0 MeV (yellow green), 4.0 MeV (blue green), 5.0 MeV (blue), and 6.0 MeV (purple). Colored arrows indicate the threshold energy $2\Delta_{\text{ext}}$ for corresponding λ_n . See text for details.

tron strength functions, Figs. 4(a)(c), that a low-lying collective state having large neutron strengths appears around 1 – 2 MeV of excitation energy in all the cases of λ_n . The transition densities of these states, shown in Fig. 5, indicate that they have the character of the AB phonon mode in the neutron gas region $r \gtrsim 8$ fm. Although admixture of the cluster shape vibration is seen in the transition densities, the proton quadrupole strength of these states is not significant (see Fig. 4(b)). Therefore all these states are interpreted as the AB-phonon-dominant mode. The excitation energy and the neutron strengths increase monotonically with increase of the neutron chemical potential λ_n .

The proton quadrupole strength, shown in Fig. 4(b), exhibits different behaviours. The low-lying collective state with enhanced proton strength are found only for $\lambda_n = 3.0$ MeV and 4.0 MeV. These are the cluster-vibration-dominant mode discussed in the subsection just above. There exists no cluster-vibration-dominant mode

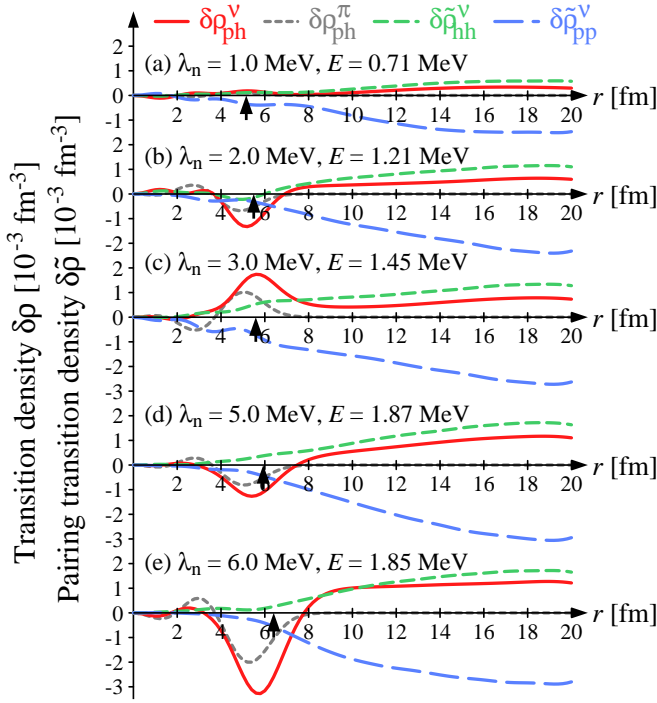


FIG. 5. Transition densities $\delta\rho_{\text{ph}}^V(r)$, $\delta\rho_{\text{ph}}^\pi(r)$, $\delta\tilde{\rho}_{\text{pp}}^V(r)$, and $\delta\tilde{\rho}_{\text{hh}}^V(r)$ of the AB-phonon-dominant-mode for $Z = 28$ systems with $\lambda_n =$ (a) 1.0 MeV, (b) 2.0 MeV, (c) 3.0 MeV, (d) 5.0 MeV and (e) 6.0 MeV. See text for details.

in the low-lying region in the cases of $\lambda_n = 2.0$ MeV, 5.0 MeV and 6.0 MeV. (In case of $\lambda_n = 1.0$ MeV, we find a state which has partial character of the cluster vibration at $E = 1.18$ MeV, which lies above the continuum threshold $2\Delta_{\text{ext}}$.)

Figure 6 shows more detailed information on the excitation energy E_{AB} of the AB-phonon-dominant mode and the energy E_{cl} of the cluster-vibration-dominant mode, plotted as a function of λ_n . The proton quadrupole strength $B(Q_p)$ of the cluster-vibration-dominant mode is also plotted. For comparison we also plot the excitation energy and $B(Q_p)$ of the 2_1^+ state of the near-drip-line nuclei $^{80-88}\text{Ni}$ which have negative λ_n .

The excitation energy E_{AB} of the AB-phonon-dominant mode has smooth dependence on λ_n . It agrees well with an hydrodynamic estimate of the excitation energy of the quadrupole AB mode, $\hbar\omega_{\text{hyd}}$, which is obtained assuming that the phonon amplitude is expressed by the spherical Bessel function, $\phi(r) \propto j_2(qr)$ with boundary condition $d\phi(r)/dr = 0$ at $r = R_{\text{WS}} = 20$ fm.¹

¹ In this estimate, we assume $\phi(r) \propto j_2(qr)$ together with the boundary condition $d\phi(r)/dr|_{r=R_{\text{box}}} = 0$. Combination of the phonon dispersion relation $\omega = c_{\text{ph}}q$ and the hydrodynamic estimate of the phonon velocity $c_{\text{ph}} = \sqrt{(\partial\lambda_n/\partial\rho)\rho/m}$ gives an estimated excitation energy $\hbar\omega_{\text{hyd}}$. Here, we use $\rho(\lambda_n)$ evaluated for uniform neutron matter with the same Skyrme functional SLy4.

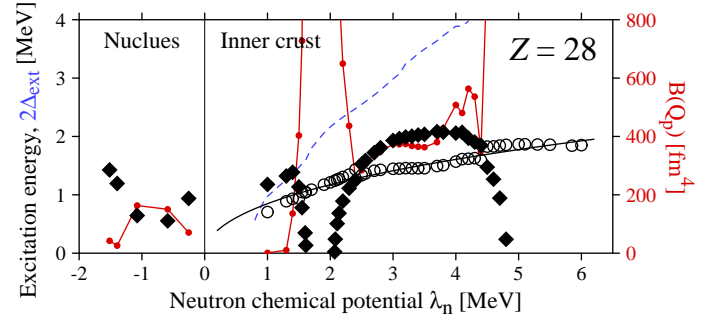


FIG. 6. Excitation energy E_{AB} of the lowest AB-phonon-dominant mode (open circle) and the energy E_{cl} of the cluster-vibration-dominant mode (filled diamond) for $Z = 28$ systems, plotted as a function of the neutron chemical potential λ_n . Blue dashed curve is the threshold energy $2\Delta_{\text{ext}}$. Red dots connected with line denote the proton quadrupole strengths $B(Q_p)$ of the cluster-vibration-dominant mode. The results for near-drip-line nuclei $^{80,82,\dots,88}\text{Ni}$ are also plotted. The thin black line is the hydrodynamic estimate $\hbar\omega_{\text{hyd}}$ of the quadrupole AB phonon mode in uniform superfluid neutron gas in the same Wigner-Seitz cell.

This indicates that the presence of the nuclear cluster affects only to a small extent the excitation energy of the AB-phonon-dominant mode. It is also consistent with our observation in Figs. 1 and 3 that the coupling between the quadrupole shape vibration of cluster and the quadrupole AB phonon is weak. For $0 < \lambda_n < 1$ MeV, we do not plot the results since the collective modes do not appear at low excitation energies below $2\Delta_{\text{ext}}$. Note however that the AB phonon mode would appear below $2\Delta_{\text{ext}}$ if we adopted a large Wigner-Seitz cell.

The cluster-vibration-dominant mode displays strong, non-monotonic and oscillatory λ_n -dependence. As λ_n increases slightly above 1.3 MeV the excitation energy E_{cl} drops off sharply. The $B(Q_p)$ value increases dramatically. This behaviour reminds us of the softening of low-lying quadrupole vibration in isolated nuclei, and the same appears to happen for the nuclear cluster in the Wigner-Seitz cell. The cluster-vibration-dominant mode is not found in the interval of $\lambda_n \approx 1.6 - 2.0$ MeV, and it suggests instability of the spherical nuclear cluster toward the quadrupole deformation. (In this case the QRPA energy of the quadrupole shape vibration is expected to be “imaginary”.) In the interval of $\lambda_n \approx 2.1 \sim 4.8$ MeV, the cluster-vibration-dominant mode emerges at finite excitation energy. The softening is seen above $\lambda_n \gtrsim 4.5$ MeV and the instability occurs again in the interval $\lambda_n \approx 4.8 \sim 6$ MeV.

Figure 7 shows the same plot as Fig. 6, but for systems with $Z = 20, 40$ and 50 . The energy of the AB-phonon-dominant mode agrees well with the hydrodynamical estimate while the strong and oscillatory λ_n -dependence of the cluster-vibration-dominant mode is present in all the cases.

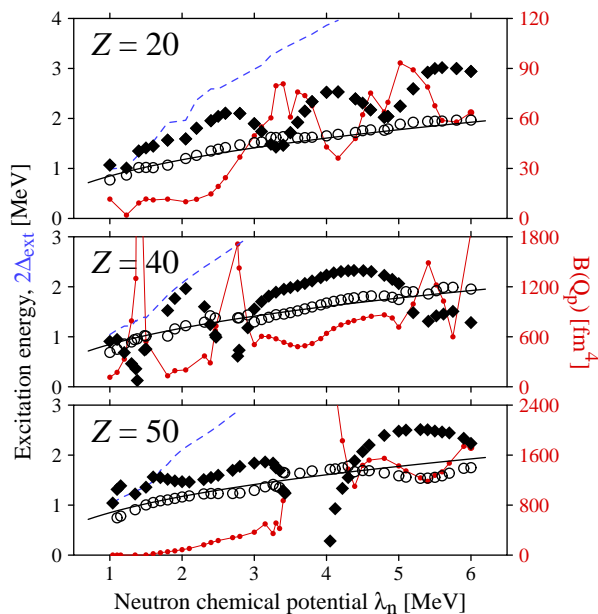


FIG. 7. The same as Fig. 6, but for systems with $Z = 20, 40,$ and 50 .

D. Resonance shell effect on cluster shape vibration

The strong and oscillatory λ_n -dependence suggests possible shell effect in the cluster-vibration-dominant mode. However, the conventional idea of the shells characterized by the magic numbers $N = 50, 82, 126,$ etc. is not appropriate here as neutron single-particle orbits around the neutron Fermi energy λ_n are unbound states having a quasi-continuum spectrum.

In order to clarify the suggested shell effect, we look into the single-particle eigenstates in the Hartree-Fock potential. Figure 8 shows the neutron and proton single-particle energies for the $Z = 28$ systems with $\lambda_n = 1.0, 2.0, \dots, 6.0$ MeV. The thick black bars connected with dashed lines denote the resonant single-particle states with quantum numbers $1h_{11/2}, 1h_{9/2}, 1i_{13/2},$ and $1i_{11/2}$. Bound high- j orbits are also connected with thin dashed lines for reference. Red horizontal bars connected with dashed line denote the neutron Fermi energy (chemical potential) λ_n , and blue bars the neutron Hartree-Fock potential U_{ext} in the region of neutron gas. The single-particle states with energy below U_{ext} are localized states bound to the nuclear cluster while those above U_{ext} are unbound states, which also have discrete energies because of the Wigner-Seitz approximation with finite cell radius. Concerning the bound single-particle states, the single-particle energy gaps at the neutron number $N = 50$ and at the proton numbers $Z = 28, 50$ and 82 are clearly visible. For unbound single-particle states, on the other hand, the single-particle energy spacings are much smaller than those of bound states, and the spacings approach zero if we take larger Wigner-Seitz radius. We have examined wave functions of all the unbound single-particle states of neutrons. Among the discretized unbound states, we find a few characteristic states whose wave function has

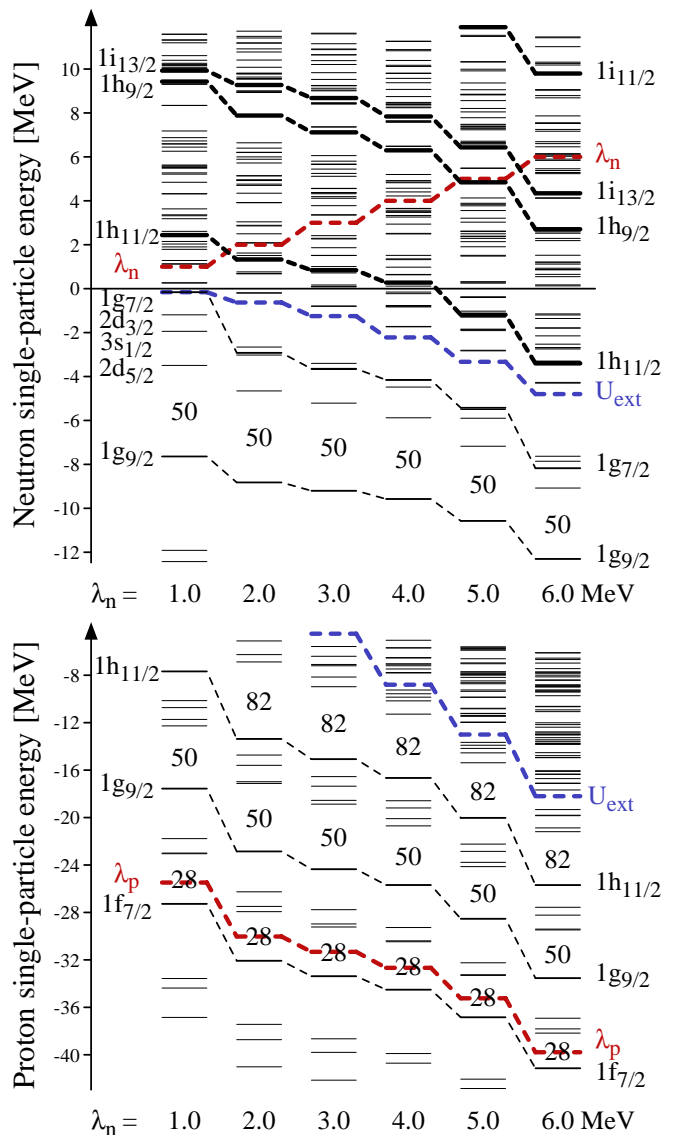


FIG. 8. (a) Neutron single-particle energies for $Z = 28$ systems with $\lambda_n = 1.0, 2.0, \dots, 6.0$ MeV. Thick black bars connected with dashed lines denote the resonant single-particle states with quantum numbers $1h_{11/2}, 1h_{9/2}, 1i_{13/2},$ and $1i_{11/2}$. Bound high- j orbits are also connected with thin dashed lines for reference. Red horizontal bars connected with dashed line denote the neutron Fermi energy (chemical potential) λ_n , and blue bars the neutron Hartree-Fock potential U_{ext} in the region of neutron gas. (b) The same as (a), but for protons. Numbers $28, 50$ and 82 inserted in levels are the spherical magic numbers.

large amplitude inside the nuclear cluster ($r \lesssim 6$ fm), at least larger than amplitude in the exterior region. Such states correspond to resonant single-particle states and they are marked with thick lines in Fig. 8(a). The resonant single-particle states are high- l orbits with no radial node inside the cluster, which can be labeled as $1h_{11/2}, 1h_{9/2}, 1i_{13/2}$ etc. Note that these high- l orbits have large

centrifugal barriers which allow resonances. The barrier height for $l = 5$ partial waves ($h_{11/2,9/2}$) is about 10 MeV in the case of $\lambda_n = 5.0$ MeV.

We found that these resonant high- l orbits are the origin of the shell effect seen in the cluster shape vibration.

Thick red bars in Fig. 8(a) indicate the neutron Fermi energy (chemical potential) λ_n . As λ_n increases, the relative position of λ_n moves upward with respect to the spectrum of unbound neutron single-particle states. Then, the neutron Fermi energy λ_n crosses with the resonant $1h_{11/2}$ neutron state at $\lambda_n \approx 1.8$ MeV while the other resonant $1h_{9/2}$ and $1i_{13/2}$ orbits crosses with λ_n at $\lambda_n \approx 5.0$ and 5.5 MeV, respectively. It is seen that the softening and the instability of the cluster shape vibration mode occurs when these crossings occur.

With these observations, we infer the mechanism of the shell effect seen in the quadrupole shape vibration of cluster. A resonant high- l orbit has wave function concentrated in the region of the nuclear cluster, and hence it may play a similar role of a single- j shell in nuclear structure problems. Furthermore we can assume that non-resonant unbound single-particle orbits do not play major roles as they are single-particle states contributing mainly to neutron gas, but not to the nuclear cluster. In this situation enhancement of the quadrupole collectivity occurs when the Fermi energy is located close to the energy of the single- j shell (the resonant high- l state in the present case) and the shell is approximately half-filled. This shell effect caused by the resonant single-particle states is very different from the conventional one, in which the shells refer to bound orbits in nuclei and the associated magic numbers 20, 28, 50, 82, etc. It also differs from the continuum shell effect[47, 48] which is present in the level density of the non-resonant unbound states. To distinguish it from the existing concepts of the shell effect, we shall call it *resonance shell effect*. Note that Baroni et al. [25] points out importance of neutron resonant high- l single-particle states as one of major contributors to the low-lying and high-lying quadrupole modes. Their discussion is related to the present resonance shell effect, but the roles of the Fermi energy and the pair correlation need to be noticed to explain the oscillatory behaviour of the quadrupole collectivity as a function of the neutron Fermi energy.

The strong and oscillatory λ_n -dependence of the cluster-vibration-dominant mode in the $Z = 20, 40$ and 50 systems, shown in Fig. 7, is also nicely explained with the resonance shell effect. The softening of the shape vibration around $\lambda_n \approx 3.3$ MeV and 4.8 MeV in the $Z = 20$ system can be related to $1g_{7/2}$ and $1h_{11/2}$ resonant states of neutrons, respectively. For the softening around $\lambda_n \approx 1.4$ MeV, 2.6 MeV and 5.4 MeV in the $Z = 40$ system, neutron $1h_{9/2}$, $1i_{13/2}$, and $1i_{11/2}$ resonant states, respectively, are the keys. The instability around $\lambda_n \approx 3.7$ MeV in the $Z = 50$ system is due to neutron $1i_{11/2}$ resonant state.

In the present study, we have analyzed the systems with $Z = 20, 28, 40$ and 50 in which the protons have

closed-shell configurations. In realistic calculations of inner crust[31, 35–37], the predicted proton number of nuclear cluster is not limited to these magic numbers, but rather the protons often have open shell configurations where the proton pair correlation also takes part in. In such cases, the quadrupole collectivity of the cluster shape vibration is even more enhanced due to the contribution of open shell protons than in the present case of proton closed shell, and there will be more possibilities of the quadrupole deformation of nuclear clusters in situations where the resonance shell effect is expected. It is also remarked that the occurrence of quadrupole-deformed nuclear cluster caused by the resonance shell effect is expected even at low densities (as well as high densities) of superfluid neutron gas. This is in contrast to the deformation mechanism originating from the Coulomb lattice energy, which is responsible for the manifestation of various pasta structures[3, 49–51]. It is interesting to explore deformed clusters at low neutron-gas densities, $0 < \rho_{n,\text{ext}} \lesssim \rho_0/10$, by means of quantum mechanical approach such as the HFB and the Bogoliubov-de-Genne-Kohn-Sham density functional models. Note that the previous HF calculations analyzing deformed clusters[48, 52–55] focus on the pasta structures in the bottom layers of inner crust where the neutron-gas density or the average baryon density is rather high $\rho \gtrsim \rho_0/10$.

IV. CONCLUSIONS

We have investigated collective excitations in the inner crust of neutron stars in the framework of the nuclear density functional theory. We consider configurations where spherical clusters are immersed in superfluid neutron gas, and describe low-lying quadrupole collective excitations around the cluster by means of the HFB plus QRPA model formulated in a spherical Wigner-Seitz cell. We adopt the Skyrme SLy4 functional and the density-dependent delta pairing interaction. Numerical analysis is performed by varying the neutron chemical potential (Fermi energy) $\lambda_n = 1 - 6$ MeV changing the density of superfluid neutrons and the proton number of the cluster.

Our calculation demonstrates that there coexist the Anderson-Bogoliubov (AB) phonon mode of neutron superfluid and the quadrupole shape vibration of the cluster, and these two fundamental modes mix with each other only weakly. The AB-phonon-dominant-mode, i.e. the AB phonon mode with small mixing of the quadrupole shape vibration of cluster, emerges systematically, and its excitation energy exhibits smooth and monotonic dependence on λ_n , which agrees fairly well with the hydrodynamical estimate of the AB phonon in uniform neutron superfluid. The results point to the weak coupling between the quadrupole AB phonon mode of neutron gas and the quadrupole shape vibration of clusters. This is consistent with our previous study[26] suggesting that the dipole AB phonon and the displace-

ment motion of clusters is weak.

Another remarkable finding is that the excitation energy of the cluster shape vibration varies in the range of 0 – 3 MeV with strong and oscillatory λ_n -dependence, in contrast to the AB phonon mode. This behavior is traced to a new kind of shell effect, named the resonance shell effect, which is associated with unbound but resonant single-particle states of neutrons orbiting around the cluster with large orbital angular momentum. The resonance shell effect causes enhancement of collectivity, softening and even instability of the quadrupole shape degrees of freedom of clusters. This suggests that occur-

rence of quadrupole-deformed nuclear cluster is possible in any layers of inner crust if the resonance shell effect induces the instability.

ACKNOWLEDGMENTS

This work was supported by JSPS KAKENHI Grant Number JP17K05436, and by Grant-in-Aid for Scientific Research on Innovative Areas, No. 24105008, by The Ministry of Education, Culture, Sports, Science and Technology, Japan.

-
- [1] N. Chamel, and P. Haensel, *Living Rev. Relativity*, **11**, 10 (2008).
- [2] P. Haensel, A. Y. Potekhin, D. G. Yakovlev, *Neutron Stars 1: Equation of State and Structure*, Astrophysics and Space Science Library, vol.326 (Springer, New York, 2007).
- [3] C. J. Pethick, D. G. Ravenhall, *Annu. Rev. Nucl. Part. Sci.* **45**, 429 (1995).
- [4] P. W. Anderson, N. Itoh, *Nature*, **256**, (1975).
- [5] M. Ali Alpar, *Astrophys. J.* **213**, 527 (1977)
- [6] D. Pines and M. Ali Alpar, in *The Structure and Evolution of Neutron Stars*, ed. D. Pines, R. Tamagaki, and S. Tsuruta (Addison Wesley, 1992), p.7.
- [7] R. C. Duncan, *Astrophys. J.* **498**, L45 (1998).
- [8] L. Samuelson, and N. Andersson, *Mon. Not. R. Astron. Soc.*, **374**, 256 (2007).
- [9] N. Andersson, K. Glampedakis, and L. Samuelsson, *Mon. Not. R. Astron. Soc.* **396**, 894 (2009).
- [10] P. W. Anderson, *Phys. Rev.* **112**, 1900 (1958).
- [11] N. N. Bogoliubov, V. V. Tolmachev, and D. V. Shirkov, *A New Method in the Theory of Superconductivity* (Academy of Science, Moscow, 1958, New York, 1959).
- [12] V. M. Galitskii, *JETP* **34**, 1011 (1958).
- [13] D. N. Aguilera, V. Cirigliano, J. A. Pons, S. Reddy, and R. Sharma, *Phys. Rev. Lett.* **102**, 091101 (2009).
- [14] C. J. Pethick, N. Chamel, and S. Reddy, *Prog. Theor. Phys. Suppl.* **186**, 9 (2010).
- [15] V. Cirigliano, S. Reddy, and R. Sharma, *Phys. Rev. C* **84**, 045809 (2011).
- [16] D. Page and S. Reddy, in *Neutron Star Crust*, ed. by C. Bertulani and J. Piekarewicz (Nova Science, 2012), p.281
- [17] N. Chamel, D. Page, and S. Reddy, *Phys. Rev. C* **87**, 035803 (2013); *J. Phys. Conf. Ser.*, **665**, 012065 (2016).
- [18] D. Kobyakov and C. J. Pethick, *Phys. Rev. C* **87**, 055803 (2013)
- [19] D. Kobyakov and C. J. Pethick, *Phys. Rev. Lett.* **112**, 112504 (2014).
- [20] N. Martin and M. Urban, *Phys. Rev. C* **90**, 065805 (2014).
- [21] E. Khan, N. Sandulescu, and N. V. Giai, *Phys. Rev. C* **71**, 042801 (R) (2005).
- [22] P. Magierski and A. Bulgac, *Acta Phys. Pol. B* **35**, 1203 (2004).
- [23] N. Martin and M. Urban, *Phys. Rev. C* **94**, 065801 (2016).
- [24] M. Grasso, E. Khan, J. Margueron, N. V. Giai, *Nucl. Phys. A* **807**, 1 (2008).
- [25] S. Baroni, A. Pastore, F. Raimondi, F. Barranco, R. A. Broglia, and E. Vigezzi, *Phys. Rev. C* **82**, 015807 (2010).
- [26] T. Inakura and M. Matsuo, *Phys. Rev. C* **96**, 025806 (2017).
- [27] M. Matsuo, *Nucl. Phys. A* **696**, 371 (2001); *Prog. Theor. Phys. Suppl.* **146**, 110 (2002).
- [28] Y. Serizawa and M. Matsuo, *Prog. Theor. Phys.* **121**, 97 (2009).
- [29] M. Matsuo and Y. Serizawa, *Phys. Rev. C* **82**, 024318 (2010).
- [30] T. Nakatsukasa, K. Matsuyanagi, M. Matsuo, and K. Yabana, *Rev. Mod. Phys.* **88**, 045004 (2016).
- [31] J. W. Negele and D. Vautherin, *Nucl. Phys. A* **207**, 298 (1973).
- [32] F. Barranco, R. A. Broglia, H. Esbensen, and E. Vigezzi, *Phys. Rev. C* **58**, 1257.
- [33] N. Sandulescu, N. V. Giai, and R.J. Liotta, *Phys. Rev. C* **69**, 045802 (2004).
- [34] N. Sandulescu, *Phys. Rev. C* **70**, 025801 (2004).
- [35] M. Baldo, U. Lombardo, E. E. Sperstein, and S. V. Tolokonnikov, *Nucl. Phys. A* **750**, 409 (2005).
- [36] M. Baldo, E. E. Sperstein, and S. V. Tolokonnikov, *Nucl. Phys. A* **775**, 235 (2006).
- [37] F. Grill, J. Margueron, and N. Sandulescu, *Phys. Rev. C* **84**, 065801 (2011).
- [38] A. Pastore, S. Baroni, and C. Losa, *Phys. Rev. C* **84**, 065807 (2011)
- [39] A. Pastore, *Phys. Rev. C* **86**, 065802 (2012).
- [40] E. Chabanat, P. Bonche, P. Heenen, J. Meyer, and R. Schaeffer, *Nucl. Phys. A* **635**, 231 (1998).
- [41] M. Matsuo, *Phys. Rev. C* **73**, 044309 (2006).
- [42] M. Matsuo, Y. Serizawa, and K. Mizuyama, *Nucl. Phys. A* **788**, 307c (2007).
- [43] E. Khan, N. Sandulescu, N. V. Giai, and M. Grasso, *Phys. Rev. C* **69**, 014314 (2004).
- [44] E. Khan, M. Grasso, and J. Margueron, *Phys. Rev. C* **80**, 044328 (2009).
- [45] N. Paar, D. Vretenar, E. Khan, and G. Colò, *Rep. Prog. Phys.* **70**, 691 (2007).

- [46] P. Ring and P. Schuck, *The Nuclear Many-Body Problem*, (Springer-Verlag, Berlin, 1980).
- [47] A. Bulgac and P. Magierski, *Nucl. Phys. A* **683**, 695 (2001).
- [48] P. Magierski and P.-H. Heenen, *Phys. Rev. C* **65**, 045804 (2002).
- [49] D. G. Ravenhall, C. J. Pethick and J. R. Wilson, *Phys. Rev. Lett.* **50**, 2066 (1983).
- [50] M. Hashimoto, H. Seki and M. Yamada, *Prog. Theor. Phys.* **71**, 320 (1984).
- [51] K. Oyamatsu, *Nucl. Phys. A* **561**, 431 (1993).
- [52] P. Gögelein and H. Mütter, *Phys. Rev. C* **76**, 024312 (2007).
- [53] W. G. Newton and J. R. Stone, *Phys. Rev. C* **79**, 055801 (2009).
- [54] H. Pais and J. R. Stone, *Phys. Rev. Lett.* **109**, 151101 (2012).
- [55] F. J. Fattoyev, C. J. Horowitz and B. Schuetrumpf, *Phys. Rev. C* **95**, 055804 (2017).